High field gradient targeting of magnetic nanoparticle-loaded endothelial cells to the surfaces of steel stents

Boris Polyak*, Ilia Fishbein†, Michael Chorny†, Ivan Alferiev†, Darryl Williams†, Ben Yellen‡, Gary Friedman§, and Robert J. Levy†¶

*Department of Surgery, Drexel University College of Medicine, Philadelphia, PA 19102; †Division of Cardiology, Children's Hospital of Philadelphia, Philadelphia, PA 19104; ‡Department of Mechanical Engineering and Materials Science, Duke University, Durham, NC 27708; and §Department of Electrical and Computer Engineering, Drexel University, Philadelphia, PA 19104

Edited by Alexander M. Klibanov, Massachusetts Institute of Technology, Cambridge, MA, and approved November 27, 2007 (received for review September 5, 2007)

A cell delivery strategy was investigated that was hypothesized to enable magnetic targeting of endothelial cells to the steel surfaces of intraarterial stents because of the following mechanisms: (*i*) preloading cells with biodegradable polymeric superparamagnetic nanoparticles (MNPs), thereby rendering the cells magnetically responsive; and (*ii*) the induction of both magnetic field gradients around the wires of a steel stent and magnetic moments within MNPs because of a uniform external magnetic field, thereby targeting MNP-laden cells to the stent wires. *In vitro* studies demonstrated that MNP-loaded bovine aortic endothelial cells (BAECs) could be magnetically targeted to steel stent wires. *In vivo* MNP-loaded BAECs transduced with adenoviruses expressing luciferase (Luc) were targeted to stents deployed in rat carotid arteries in the presence of a uniform magnetic field with significantly greater Luc expression, detected by *in vivo* optical imaging, than nonmagnetic controls.

cell therapy | gene therapy | local delivery | nanotechnology

Cell therapy represents a forefront approach with great promise. In particular, reendothelization of diseased or injured arteries is a goal of endothelial-related cell therapies (1, 2). However, there is a paucity of delivery strategies for localizing cell therapy to target sites (1, 2). The present studies report an approach for delivering endothelial cells to intravascular steel stents. Balloon-deployable stents are now the treatment of choice for vasoocclusive disease. Advanced stent designs with drug-eluting capabilities have resulted in a paradigm shift in the care of coronary disease (3–6). However, the lack of reendothelization (1, 2) after stent angioplasty remains an unsolved problem (3–6). Stents are commonly composed of steel alloys, such as the medical-grade stainless-steel 316L, which exhibits a minimal response to external magnetic fields. However, we hypothesized that by using a more magnetically responsive alloy, such as a 304-grade stainless steel, instead of 316L, it would be possible to locally deliver genetically modified endothelial cells to stent surfaces by using magnetic gradient-related mechanisms.

Previous investigations of magnetically targeted cell-delivery systems, which have all exclusively used locally applied magnets, rather than uniform magnetic fields, have been hampered by a number of factors. These studies by others (7–9) have used nonbiodegradable magnetic nanoparticles that cannot be removed from the tissue after delivery. More fundamentally, these previous studies used magnetic field sources in a suboptimal manner. Thus, prior work has been limited to using a single source of magnetic field, in which either a locally applied permanent magnet (7, 8) or a ferromagnetic medical implant (9) was used to implement the magnetic capture system. Such sources can be designed to increase the magnetizing field of cells loaded with magnetic nanoparticles or the field gradient, but not both, making it impossible to maximize the fraction of captured nanoparticle-loaded cells by these techniques. Our concept is fundamentally different, compared with these alternative approaches, in that we hypothesize that the magnetic force can be maximized by using a relatively strong uniform field to magnetize the magnetic nanoparticle-loaded cells, and this effect also is superimposed on high-level magnetic gradients within the steel stent wire network induced by the presence of a uniform field. Specifically, a uniform magnetic field is supplied by electromagnetic coils positioned external to the body, and the short-range, high-gradient magnetic fields are produced by the magnetizable wires of a stent for the purpose of maximizing the regional magnetic force on endothelial cells loaded with magnetic nanoparticles (Fig. 1). In practice, this technique enables a far greater fraction of the delivered materials to be captured than if a single source magnetic field were used.

To examine this concept experimentally, we first formulated and characterized biodegradable polymeric superparamagnetic nanoparticles (MNPs). We then identified optimal MNP cell-loading conditions with respect to MNP dose, loading time, and cell viability. We examined *in vitro* the possibility of targeting of MNP-loaded cells to the steel surfaces of stents in a model flow-loop system in the presence of uniform magnetic fields by using paired electromagnets. We then investigated this strategy *in vivo* in rats by using magnetic gradient-based targeting of MNP-loaded cells to the steel surfaces of intraarterial stents in the presence of a uniform magnetic field.

Results

Polylactide MNPs were prepared by a modified emulsification-solvent evaporation methodology (10) with the incorporation of oleate-coated iron oxide nanocrystals (10, 11) by using BSA as a surface-stabilizing agent. Albumin-stabilized MNPs displayed a narrow size distribution, with an average diameter of 290 ± 15 nm (Fig. 2*a*), and they exhibited superparamagnetic behavior showing no significant hysteresis and a remnant magnetization on the order of 0.5% of the saturation magnetization value (Fig. 2*b*). The stent material used was 304-grade stainless steel, which was chosen for its combination of suitable magnetic properties and its corrosion resistance in aqueous environments. The 304-grade stents also exhibited nearly superparamagnetic behavior showing only slight magnetic hysteresis and displaying a

Author contributions: B.P. and I.F. contributed equally to this work; B.P., I.F., M.C., I.A., G.F., and R.J.L. designed research; B.P., I.F., M.C., I.A., D.W., and R.J.L. performed research; B.P., M.C., I.A., B.Y., and G.F. contributed new reagents/analytic tools; B.P., I.F., M.C., I.A., B.Y., G.F., and R.J.L. analyzed data; and B.P., I.F., M.C., I.A., D.W., B.Y., G.F., and R.J.L. wrote the paper.

The authors declare no conflict of interest.

This article is a PNAS Direct Submission.

¶To whom correspondence should be addressed. E-mail: levyr@email.chop.edu.

© 2008 by The National Academy of Sciences of the USA

www.pnas.org/cgi/doi/10.1073/pnas.0708338105

Downloaded at Palestinian Territory, occupied on December 19, 2021

www.manaraa.com

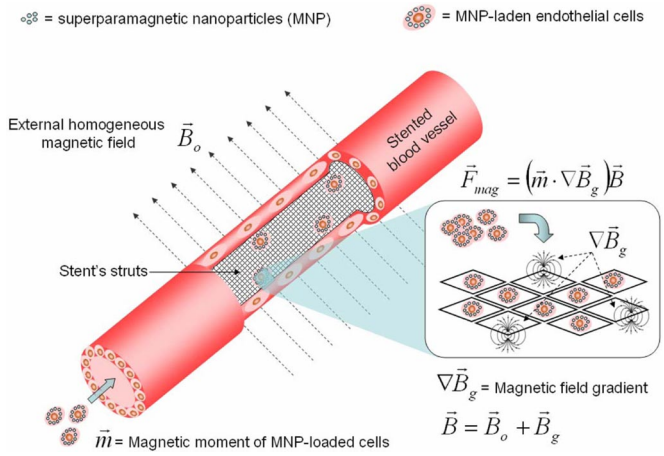

Fig. 1. A schematic representation of a stented blood vessel showing that magnetically responsive cells are attracted to steel stent struts in a uniform, magnetic field because of a generated magnetic force ($\vec{F}_{mag}$) that directly depends on the strength of the total magnetic field ($\vec{B}$), high field magnetic gradients ($\nabla \vec{B}_g$) induced on the stent struts, and the magnetic moments ($\vec{m}$) induced on MNP-loaded cells by the uniform magnetic field $\vec{B}_0$. The total magnetic field ($\vec{B}$) is a sum of a gradient field ($\vec{B}_g$) of the stent and a uniform field ($\vec{B}_0$). The steel mesh structure of the stent is shown in both the open stented blood vessel fragment and as individual strut areas in *Inset*.

remnant magnetization on the order of 7% of the saturation magnetization value (Fig. 2*c*). 316L-grade stainless-steel stents also were tested, but were not included in targeting studies because of their less responsive magnetic properties (Fig. 2*c*).

A subset of MNPs was formulated with polylactic acid (PLA) that was covalently modified with BODIPY 564/570 (12), thereby resulting in MNPs that could be used in fluorescent microscopy experiments and fluorometry-based quantitation studies. This formulation was used to characterize the kinetics of cell loading with MNPs. Bovine aortic endothelial cells (BAECs) in confluent cell cultures were incubated with various doses of BODIPY 564/570 MNP on a cell culture magnet (see *Materials and Methods*). The MNP uptake was determined at different time points by measuring the fluorescence of internalized nanoparticles. The amount of MNP internalized because of magnetic field exposure linearly depends on the MNP dose in the tested range (Fig. 2*d*). That is, ≈30% of internalization was observed after 8 h, and the uptake was essentially complete after 24 h (Fig. 2 *d* and *e*). Cell viability was not adversely affected by internalized MNPs, as assessed by the results of Calcein green staining and Alamar blue assays (Fig. 2 *e* and *f*, respectively). Cell survival of 83 ± 3% relative to untreated cells was observed at the highest applied MNP dose (9 μg per well, corresponding to a MNP loading of 0.3 ng per cell) and at the maximal incubation time of 24 h (Fig. 2*f*). Based on these results, we chose an MNP dose of 0.2 ng per cell for subsequent experiments (92 ± 2% cell survival; a dose of 5.8 μg per well per Fig. 2*f*). As expected, BAECs laden with MNPs demonstrated superparamagnetic behavior showing hysteretic properties similar to free (noncell-associated) MNPs (i.e., a remnant magnetization of <1% of the saturation value) (Fig. 2*g*).

MNP-loaded endothelial cell targeting to 304-grade stainless-steel stents was first studied in a model flow-loop system. In the absence of an externally applied uniform magnetic field, almost no cell capture was observed (Fig. 3*a*). However, when a uniform magnetic field was applied across the stent within the flow-loop system, the stent captured a significant percentage of the circulating cells, demonstrating an initial rate of 1% of cells captured per min (Fig. 3*a*). Saturation in cell capture was observed within 50 min after the magnetic field was applied, resulting in the targeting of 20% of the circulating cells (≈0.5 × 10^6). That is, ≈50% of the captured cells (≈0.25 × 10^6) accumulated on the stent surface within the first 6 min. Fig. 3*b* shows the stent surface at the end of the experiment with adherent cells completely covering the stent wire surfaces, as demonstrated by red MNP fluorescence microscopy results and Calcein green staining, indicating viability of the captured cells (Fig. 3*c*).

Acute rat carotid-stenting studies (13, 14) were carried out by transthoracic injection of BAECs loaded with MNPs into the left ventricular cavity in the presence of a uniform magnetic field (1,000 G) across the region of the stented artery (Fig. 3 *d* and *e*). The animals were killed 5 min after magnetic targeting, and the stents were retrieved, revealing targeting of MNPs to 304-grade stainless-steel stent surfaces in the presence of a magnetic field (Fig. 3*d*), again with complete uniform coverage of the stent wires with cells containing fluorescent MNPs. However, in the absence of a magnetic field, no detectable MNP-loaded BAECs were demonstrable (Fig. 3*e*). Thus, these short-term *in vivo* results were comparable to the *in vitro*-targeting studies (Fig. 3*b*).

We next carried out experiments by using BAECs both loaded with MNPs and transduced with luciferase (Luc)-encoding, replication-defective adenoviruses (AdLuc). Our initial studies examined magnetic targeting of MNP-loaded, Luc-modified BAECs with local delivery in a stop-flow setting (Fig. 3*f*), using Luc transgene activity as an endpoint, and detected with intravital bioluminescence imaging (Fig. 3*f*). After *in vitro* AdLuc transduction and preloading with MNPs, BAECs were harvested and locally delivered to an isolated stented segment of each rat's carotid artery in the presence or absence of a magnetic field (Fig. 3*f*). The stented vessel was temporarily tied off at both ends (stop-flow delivery technique), whereas the MNP-loaded BAECs were delivered to the stented section for 15 s (Fig. 3*f*). The cell suspension was then evacuated from the artery, and the magnetic field was maintained for an additional 5 min before the circulation was allowed to resume. The animals were recovered and studied 48 h later; as expected, significantly greater transgene expression ($P = 0.045$) was demonstrated by using local perivascular luciferin administration, followed by bioluminescent *in vivo* optical imaging in animals that had been administered with MNP-loaded BAECs in the presence of a uniform magnetic field, compared with a control group not subjected to magnetic delivery conditions (Fig. 3*f*). It also is noteworthy that bioluminescent whole-body imaging scans of the animals in these studies revealed an absence of transgene activity except within the stented carotid segments (data not shown).

Magnetically targeted delivery of MNP-loaded BAECs without interruption of the stented carotid blood flow also was investigated by injecting the MNP-loaded BAECs expressing Luc over the course of 1 min through a catheter positioned in the aortic arch with exposure to a uniform magnetic field for 5 min (Fig. 3*g*). Specific targeting to the deployed stents due to the applied field was demonstrated after 48 h by bioluminescent imaging (Fig. 3*g*), with no detectable Luc activity present in stented arterial segments that were not exposed to a magnetic field ($P = 0.005$). Furthermore, although our imaging procedures also involved entire body scans looking for Luc activity, there was an absence of bioluminescence in distal sites (data not shown) in these studies as well. Luc-positive immunostaining confirmed the presence of transgene activity in the intimal and medial regions of the stented arterial segments that were exposed to magnetic cell targeting (data not shown).

Discussion

These results demonstrate the successful targeting of magnetically responsive MNP-loaded endothelial cells to the steel surfaces of intraarterial stents by using the stent-associated magnetic field gradients resulting from the presence of an external uniform magnetic field. Virtually all previous research on this

Downloaded at Palestinian Territory, occupied on December 19, 2021
www.manaraa.com

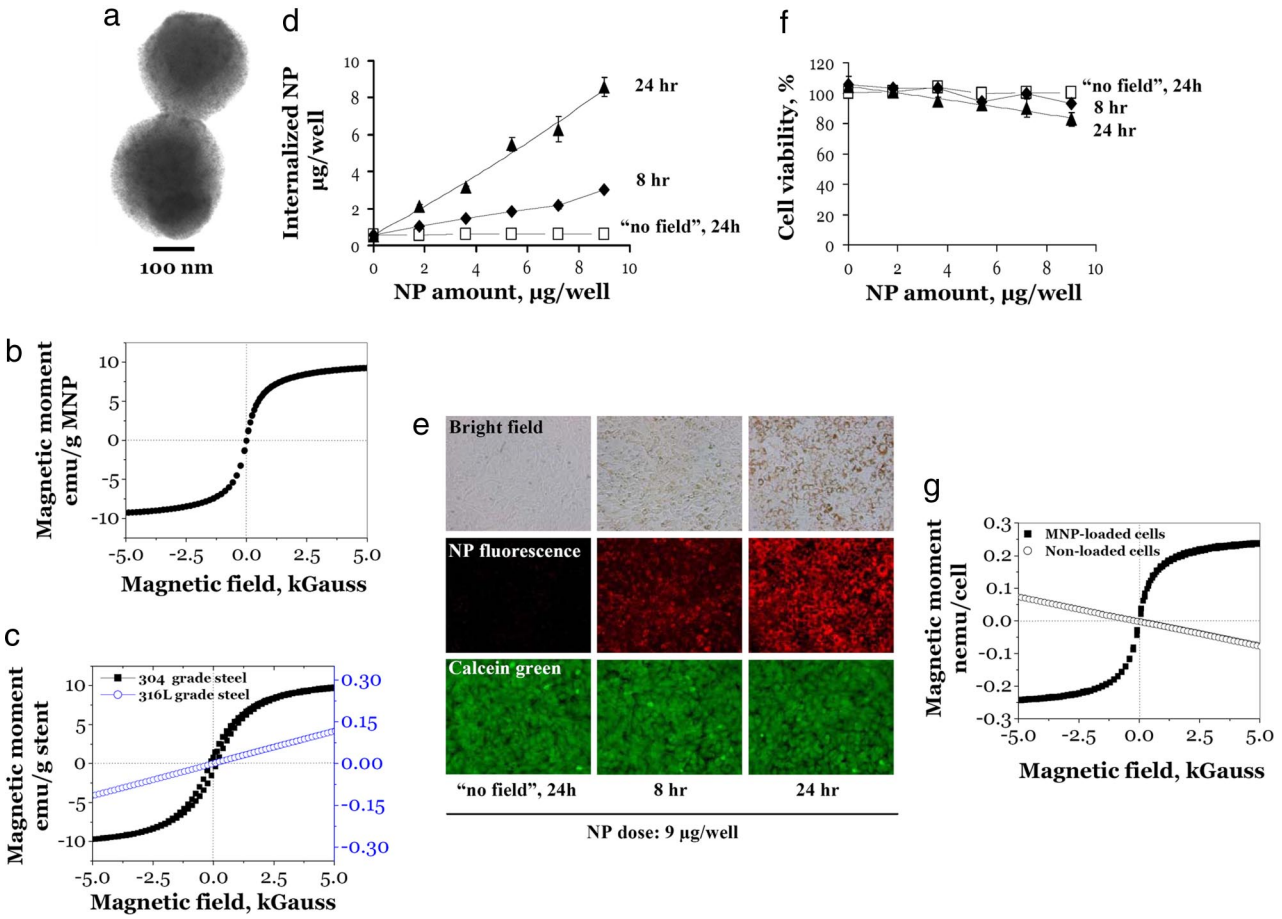

Fig. 2. Characterization of MNP and MNP-cell loading. (*a*) Transmission EM of albumin-stabilized MNPs. Note the small size and the large number of individual oleic acid-coated magnetite grains distributed in the MNP polylactide–polymeric matrix. (*b*) Magnetization curve of MNPs, which exhibit superparamagnetic behavior showing no significant hysteresis and a remnant magnetization on the order of 0.5% of the saturation magnetization value. (*c*) Magnetization curves of 304-grade (left-sided *y* axis) and 316L-grade (right-sided *y* axis) stainless-steel stents. The 304-grade stainless-steel stent exhibits a near superparamagnetic behavior showing slight hysteresis and a remnant magnetization on the order of 7% of the saturation magnetization value. By comparison, the 316L-grade stent shows far less magnetic responsiveness. (*d*) MNP-cell loading studies. The kinetics of MNP uptake by BAECs in culture as a function of MNP dose, incubation time, and the presence or absence of a magnetic field of 500 G by using a fixed magnet applied directly to the underside of the cell culture plates. The MNP uptake was determined by fluorescence of internalized MNPs. (*e*) Micrographs of BAECs in culture with bright field and red fluorescent images qualitatively showing the relative amount of MNPs internalized within cells at different time points at the applied MNP dose of 9 μg per well. Green fluorescent micrographs show cell viability as assessed by Calcein green staining. (Magnification: $\times$100.) (*f*) Cell viability as a function of MNP dose and incubation time as determined by Alamar blue assays. (*g*) Magnetization curve of BAECs loaded with MNPs demonstrates superparamagnetic behavior showing no significant hysteresis and a remnant magnetization on the order of $<$1% of the saturation magnetization value. Cells not loaded with MNPs exhibit diamagnetic behavior.

subject, whether concerned with either magnet targeting of particles or cells, has involved the use of a single magnetic field source (7–9, 15–21), rather than a homogeneous magnetic field, as used in the present experiments. However, this single-source capture method used in previous studies by others (7–9, 15–21) is at odds with the underlying physical mechanism of magnetic carrier capture, which depends on the presence of both strong far-reaching magnetic fields to magnetize the carriers (e.g., cells loaded with MNPs) and strong magnetic field gradients to apply forces on those carriers. The differences between the previous approaches that used a single magnetic field source with the current approach can be further illustrated by using the following arguments (Fig. 1). The magnetic force on MNP-loaded cells is $\vec{F}_{\text{mag}} = (\vec{m} \cdot \nabla)B$, where m is the magnetic moment and B is the external magnetic field. Suppose first that the external magnetic field $\vec{B} = \vec{B}_{\text{g}}$ is the gradient field produced by an isolated magnetic pole source. In this case, the gradient field decays inversely with the square of the distance from source, i.e., $\vec{B}_{\text{g}} \approx (1/r^2)$. The gradient of this field decays with the cube of the distance from the source, i.e., $\nabla\vec{B}_{\text{g}} \approx (1/r^3)$. If the same field is used to magnetize the MNP-loaded cells at some distance from the source, the magnetic moment decays as the field does, i.e., $\vec{m} \approx (1/r^2)$. Substituting these terms into the magnetic force expression, one obtains a force that decays inversely with the fifth power of the distance from the source, i.e., $\vec{F}_{\text{mag}} \approx (1/r^5)$. However, if the total magnetic field is a sum of gradient and uniform fields $\vec{B} = \vec{B}_{\text{g}} + \vec{B}_0$, even sufficiently far away from the gradient source, the MNP-loaded cells' magnetic moments remain independent of the distance from this source. In other words, even far away from the gradient source, where the gradient field is weak, the MNP-loaded cells are magnetized by the uniform field $\vec{B}_0$. In this case, the magnetic force decays as does the gradient of the field, i.e., $\vec{F}_{\text{mag}} \approx (1/r^3)$. It is this reduced decay of the magnetic force that permits the capture of MNP-loaded cells much farther away from the gradient source and that is the main advantage of the magnetic capture approach presented herein, which relies on the presence of both the gradient and the uniform magnetic field.

The biodegradability and biocompatibility of the PLA MNP formulation used in the present studies are well documented and

Downloaded at Palestinian Territory, occupied on December 19, 2021
www.manaraa.com

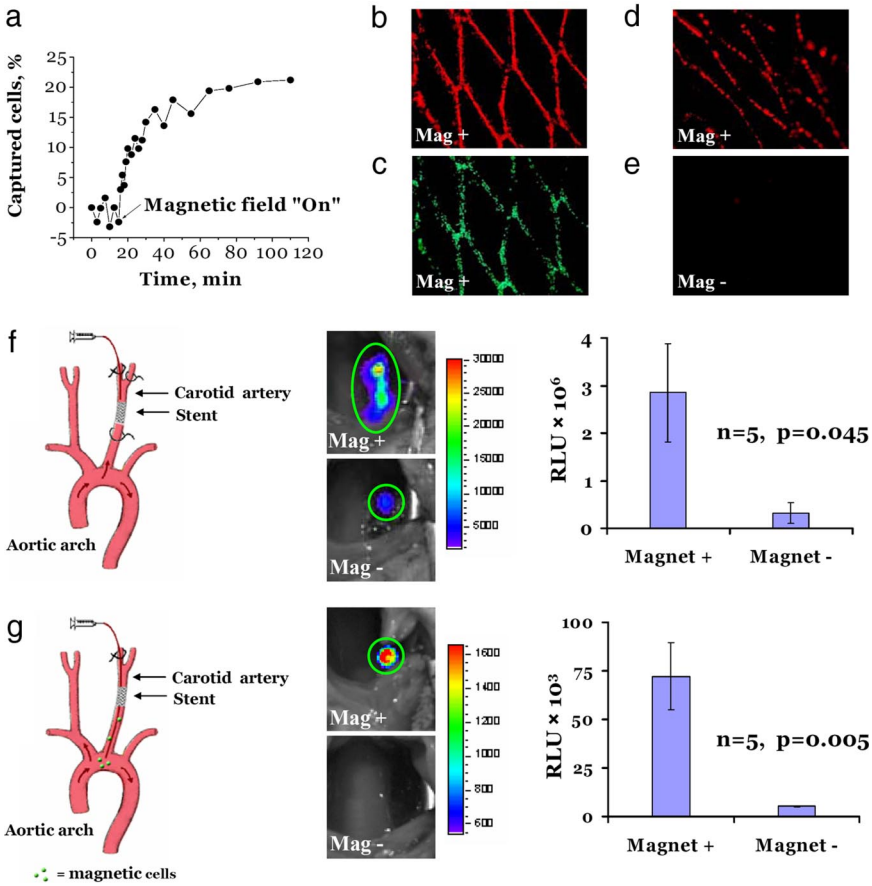

Fig. 3. Magnetic targeting of MNP-preloaded BAECs under flow conditions *in vitro* and *in vivo*. (*a*) *In vitro* capture kinetics of magnetically responsive BAECs onto a 304-grade stainless-steel stent in the presence of a uniform field of 1,000 G and a nonpulsatile flow rate of 30 ml/min. The initial capture rate was estimated to be 1% of cells per min. The data were obtained by measuring the fluorescence of MNPs. (*b* and *c*) Magnetically responsive BAECs captured *in vitro* onto a 304-grade stainless-steel stent as evidenced by the red fluorescence of MNPs (*b*) and Calcein green staining of live cells (*c*). (*d*) MNP-loaded BAECs captured *in vivo* onto a deployed 304-grade stainless-steel stent in the rat carotid artery. BAECs preloaded with fluorescent MNPs were transthoracically injected into the left ventricular cavity. Animals were exposed to a magnetic field of 1,000 G for 5 min, including the period of injection. The animals were killed 5 min after delivery, and the explanted stents were immediately examined by fluorescence microscopy. (*e*) Control rats underwent an identical procedure where no magnetic field was used. (Magnification: *b*–*e*, ×40.) (*f*) *In vivo* local magnetic cell delivery in a rat carotid stenting model under stop-flow conditions. A catheter was introduced via the external carotid into the common carotid artery and was positioned distal to a deployed stent. The cell suspension was delivered into isolated arterial segments for 15 s. (*g*) *In vivo* cell delivery under uninterrupted blood-flow conditions. A catheter was introduced via the external carotid into the common carotid and advanced beyond the stent to the aortic arch. The cells were injected at this site at the rate of 1 ml/min for 1 min. For both delivery protocols (*f* and *g*) in the magnetic group (Mag+), the injection was carried out with animals placed in a magnetic field of 1,000 G, and the field was maintained for a total of 5 min after delivery. In control rats (Mag− group), no magnetic field was applied. In both settings, BAECs were first transduced in culture with AdLuc and then loaded with MNPs. The animals were imaged 48 h after delivery by local perivascular administration of luciferin admixed in a pluronic gel. The signal emitted from the stented arterial segment due to the luciferase transgene expression was significantly higher in the animals that received cells in the presence of a magnetic field (Mag+ group).

described elsewhere (11, 22). Iron oxide, at the levels incorporated into our MNPs, is nontoxic, biocompatible, and routinely used as a contrast agent for MRI in human subjects (23). At our selected MNP loading of 0.2 ng per cell for the present *in vivo* experiments, MNP-laden cells demonstrated viability results that did not differ significantly from the control (Fig. 2*f*). Thus, it is unlikely that the levels of magnetite loading reported herein would adversely influence endothelial cell proliferation *in vivo*, although potential toxicity remains to be investigated. Furthermore, intracellular trafficking of MNPs has been reported by our group with respect to the rapid uptake and processing of MNP-delivered plasmid DNA (11). However, the fate of MNPs over time with respect to degradation and exocytosis (24) has not been studied as yet by our group or others and should be the subject of MNP investigations. Nonlocalized nanoparticles would likely be rapidly cleared by the reticuloendothelial system (25).

A number of important factors need to be addressed in studies concerning *in vivo* investigations of this approach. It is of interest that, despite the fact that a stent has a relatively small surface area, estimated to be ≈42–47 mm^2 in the present studies, our results show that even the rat carotid stents used in our experiments can be magnetically targeted with ≈10^6 MNP-loaded endothelial cells. It is noteworthy that local delivery of endothelial cells even at this level may be efficacious based on the work of others (26). Kong and coworkers (26) reported that local delivery (without magnetic localization) of 10^6 autologous endothelial progenitor cells overexpressing endothelial nitric oxide synthase in balloon-injured rabbit carotid arteries resulted in an inhibition of neointimal hyperplasia. Furthermore, our *in vitro*-modeling results (Fig. 3*a*) indicate that, although MNP-loaded cells begin to bind immediately to steel surfaces in the presence of a homogenous magnetic field, a steady-state equilibrium is reached after 20 min with documented viability (Fig. 3*a*). Thus, these data, as well as our successful *in vivo* results, provide the basis for further studies concerning the kinetics of MNP cell targeting and adhesion.

MEDICAL SCIENCES
Downloaded at Palestinian Territory, occupied on December 19, 2021
www.manaraa.com

Translating the results of the present studies into a clinical configuration to provide a homogeneous magnetic field in the region of a deployed stent could involve either (*i*) the regional application of large fixed magnets, or (*ii*) carrying out the targeting procedures in an MRI device. Our data (Fig. 2) demonstrate that ≈80–90% of the magnetic moment saturation for stents, MNPs, and MNP-loaded cells occurs in a range of 1–2 kGauss (0.1–0.2 Tesla). Thus, for example, a typical MRI system with a uniform magnetic field in the 1- to 3-Tesla range should hypothetically enable MNP cell targeting to a steel stent in the human heart. Furthermore, although the iron oxide loadings used in the present studies were demonstrated to be nontoxic *in vitro* (Fig. 2*f*), the *in vivo* use of MNP-loaded cells requires that iron dosing be monitored. However, scaling up MNP-laden cell delivery for human applications with 0.2 ng of iron oxide per cell, as in the present studies, would result in systemic exposure of a human subject receiving 10^6 to 10^7 MNP-loaded cells to iron levels ≥5,000-fold below those demonstrated by others (23) to be safe for human subjects.

It is concluded that cell targeting mediated by mechanisms elaborated on in this article, involving a complex interaction of ferromagnetic implants, MNP-loaded cells, and the presence of high field gradients because of a homogeneous magnetic field, represents a powerful strategy for the site-specific delivery of cell-based therapies. Although our example only focused on this approach by using steel stents deployed in arteries, other relevant configurations could include the use of steel stents for esophageal disorders including cancer, urinary tract stents, bile duct stenting, and the use of stents for symptomatic relief of bronchial carcinoma. Steel implants also are used extensively in orthopedic procedures and in this setting represent another hypothetical example of a potential therapeutic platform for use with magnetic cell targeting.

Materials and Methods

Nanoparticle Formulation and Characterization. Magnetite prepared from ferric and ferrous chloride (300 and 150 mg, respectively) by alkaline precipitation with aqueous sodium hydroxide was magnetically separated, resuspended in 2 ml of ethanol, and coated with 200 mg of oleic acid with heating under argon to 90°C in a water bath for 5 min. Excess oleic acid was phase-separated by dropwise addition of 4 ml of water, and the lipid-coated magnetite was washed twice with ethanol. Lipophilic magnetite was dispersed in 6 ml of chloroform, forming a stable ferrofluid. The resulting organic dispersion of iron oxide was used to dissolve PLA, thus forming an organic phase. The organic phase was emulsified in an aqueous albumin solution (1%) by sonication in an ice bath, followed by organic solvent evaporation. The particles were separated from the unbound albumin by repeated magnetic sedimentation/resuspension cycles and lyophilized with 5% (wt/vol) glucose as a cryoprotectant. Lyophilized MNP were kept at −20°C and resuspended in deionized water before use.

Particle size measurements were performed by using the 90 Plus Particle Size Analyzer (Brookhaven Instruments). The magnetic properties of MNPs and cells loaded with MNP were estimated from the hysteresis curves of either MNP or MNP-loaded cells (5-μl samples) air-dried on a 4 × 4-mm^2 cover-glass slide by using an alternating gradient magnetometer (Princeton Instruments).

Cell Preparations. BAECs were seeded on clear-bottom 96-well plates at a density of 1.5×10^4 cells per well by using DMEM supplemented with 10% FBS for the cell-loading and cell-viability experiments. To synchronize cell cultures with respect to MNP uptake, the cells were incubated at 4°C for 30 min. Then MNP were added to cells at different doses, and cell cultures were incubated on a magnetic separator adapted for cell culture plates by using a magnetic field source of 500 G (LifeSep 96F; Dexter Magnetic Technologies). Further, at predetermined time points, cells were washed with PBS, and the amount of internalized MNP was measured fluorimetrically ($\lambda_{em}/\lambda_{ex}$ = 540/575 nm). Cell viability was determined at all time points by using Calcein green staining and the Alamar blue assay as described by the manufacturer (Biosource).

For the studies of *in vitro* cell capture on stents, BAECs were seeded on clear-bottom 12-well plates. Cells and MNPs were incubated on a magnetic source (Life Sep 96F) for 24 h to allow nearly complete (≈95%) internalization of MNPs. Then cells were trypsinized and resuspended in a cell culture medium for further magnetic capturing experiments. Cells used for *in vivo*-delivery experiments were first transduced with replication-defective type 5 (E1- and E3-deleted) AdLuc under the control of the human cytomegalovirus promoter (Gene Vector Core, University of Pennsylvania, Philadelphia, PA) for 10 h (moi = 500) and then loaded with MNPs for 24 h.

***In Vitro* and *in Vivo* Short-Term Cell-Capture Experiments.** In an *in vitro* cell-capture experiment, MNP-loaded BAECs (≈2.5×10^6) circulated in a closed-loop system, including a 304-grade stainless-steel stent (Circle Medical Devices), at a flow rate of 30 ml/min while a homogeneous magnetic field of 1,000 G was applied. A homogeneous magnetic field was produced by passing an electrical current through serially connected solenoid coils with iron cores (40 mm in diameter) placed at both sides of either a stent positioned in a flow chamber of a model loop-circulatory system or a stented animal within a distance of 40 mm between the electromagnets' cores. An electrical current of 9.4 A was generated by an HP 6034 A (Hewlett Packard) power supply by applying 28 V. The magnetic field strength was measured by a Hall Probe purchased from Lake Shore Cryotronics. Cell depletion was monitored by measuring MNP fluorescence, and the results were calculated as a percentage of captured cells.

In *in vivo* cell-capture experiments, 304-grade stainless-steel stents were deployed in the rat carotid arteries under general anesthesia (13). For acute studies, BAECs (10^6 cells in 1 ml of media) preloaded with fluorescent MNPs were transthoracically injected into the left ventricular cavity. Animals were exposed to a magnetic field of 1,000 G for 5 min by using the system described in *Cell Preparation*, including the period of injection. Control rats underwent an identical procedure, where no magnetic field was used. The animals were killed 5 min after delivery, and the explanted stents were examined by fluorescence microscopy.

Angioplasty and *in Vivo* Delivery Procedure: 48-Hour Studies. Under general anesthesia (13), the left common carotids of 450- to 500-g Sprague–Dawley male rats were injured by four passages of a Fogarty catheter before deployment (16 atm) of 304-grade stainless steel. In the model studies of cell delivery under stop-flow conditions, 23-gauge tubing was introduced via the external carotid into the common carotid artery and was positioned distal to the deployed stent. Thus, for these studies with temporary interruption of carotid blood flow, a 15-mm segment of common carotid artery encompassing the stented site was isolated by ligatures. The cell suspension of BAECs (10^6 cells per ml, with 50 μl injected) was delivered into the isolated arterial segment for 15 s, after which the excess cells that were not retained in the artery were evacuated by syringe. In studies of cell delivery under uninterrupted flow, 26-gauge tubing was introduced via the external carotid into the common carotid and advanced beyond the stent to the aortic arch. The cells were injected at the rate of 1 ml/min for 1 min. For both delivery protocols, in the magnetic (Mag+) group, the injection was carried out with animals placed in a magnetic field of 1,000 G, as described above, and the field was maintained for a total of 5 min after delivery. In control rats (Mag− group), no magnetic field was applied.

Forty-eight hours after magnetic cell delivery, all animals were subjected to bioluminescence imaging (IVIS 100; Xenogen) to detect Luc transgene activity. Imaging procedures involved local application under general anesthesia of 2.5 mg of luciferin dissolved in 250 μl of 25% Pluronic F127 (Sigma–Aldrich) gel (27) applied to the external surface of the stented common carotid artery with bioluminescence data acquisition after 5 min; both local carotid images and whole-body scans were assessed. The integration time was 10 min.

Statistical Analysis. Experimental data were presented as means ± SE. Student's *t* test was used to analyze the significance of differences in datasets. Differences were termed significant at $P < 0.05$.

ACKNOWLEDGMENTS. We thank Christina Zalite for assistance with the illustrations. This work was supported by National Institutes of Health Grant HL72108, the Nanotechnology Institute, and both the William J. Rashkind Endowment and Erin's Fund of the Children's Hospital of Philadelphia.

1. Varenne O, Pislaru S, Gillijns H, Van Pelt N, Gerard RD, Zoldhelyi P, Van de Werf F, Collen D, Janssens SP (1998) *Circulation* 98:919–926.
2. Gulati R, Jevremovic D, Peterson TE, Witt TA, Kleppe LS, Mueske CS, Lerman A, Vile RG, Simari RD (2003) *Circulation* 108:1520–1526.
3. Fattori R, Piva T (2003) *Lancet* 361:247–249.
4. Kipshidze NN, Tsapenko MV, Leon MB, Stone GW, Moses JW (2005) *Exp Rev Cardiovasc Ther* 3:953–968.
5. Burt HM, Hunter WL (2006) *Adv Drug Deliv Rev* 58:350–357.
6. Serruys PW, Kutryk MJ, Ong AT (2006) *N Engl J Med* 354:483–495.
7. Consigny PM, Silverberg DA, Vitali NJ (1999) *J Vasc Interv Radiol* 10:155–163.

Downloaded at Palestinian Territory, occupied on December 19, 2021
www.manaraa.com

8. Pislaru SV, Harbuzariu A, Agarwal G, Witt T, Gulati R, Sandhu NP, Mueske C, Kalra M, Simari RD, Sandhu GS (2006) *Circulation* 114:1314–1318.
9. Pislaru SV, Harbuzariu A, Gulati R, Witt T, Sandhu NP, Simari RD, Sandhu GS (2006) *J Am Coll Cardiol* 48:1839–1845.
10. Quintanar-Guerrero D, Allemann E, Fessi H, Doelker E (1998) *Drug Dev Ind Pharm* 24:1113–1128.
11. Chorny M, Polyak B, Alferiev IS, Walsh K, Friedman G, Levy RJ (2007) *FASEB J* 21:2510–2519.
12. Chorny M, Fishbein I, Alferiev IS, Nyanguile O, Gaster R, Levy RJ (2006) *Mol Ther* 14:382–391.
13. Fishbein I, Alferiev IS, Nyanguile O, Gaster R, Vohs JM, Wong GS, Felderman H, Chen IW, Choi H, Wilensky RL, Levy RJ (2006) *Proc Natl Acad Sci USA* 103:159–164.
14. Finn AV, Gold HK, Tang A, Weber DK, Wight TN, Clermont A, Virmani R, Kolodgie FD (2002) *J Vasc Res* 39:414–425.
15. Alexiou C, Arnold W, Klein RJ, Parak FG, Hulin P, Bergemann C, Erhardt W, Wagenpfeil S, Lubbe AS (2000) *Cancer Res* 60:6641–6648.
16. Alexiou C, Jurgons R, Schmid RJ, Bergemann C, Henke J, Erhardt W, Huenges E, Parak F (2003) *J Drug Target* 11:139–149.
17. Alexiou C, Jurgons R, Schmid R, Erhardt W, Parak F, Bergemann C, Iro H (2005) *Hno* 53:618–622.
18. Lubbe AS, Bergemann C, Huhnt W, Fricke T, Riess H, Brock JW, Huhn D (1996) *Cancer Res* 56:4694–4701.
19. Leakakos T, Ji C, Lawson G, Peterson C, Goodwin S (2003) *Cancer Chemother Pharmacol* 51:445–450.
20. Goodwin SC, Bittner CA, Peterson CL, Wong G (2001) *Toxicol Sci* 60:177–183.
21. Mah C, Fraites TJ, Jr, Zolotukhin I, Song S, Flotte TR, Dobson J, Batich C, Byrne BJ (2002) *Mol Ther* 6:106–112.
22. Shive MS, Anderson JM (1997) *Adv Drug Del Rev* 28:5–24.
23. Weissleder R, Stark DD, Engelstad BL, Bacon BR, Compton CC, White DL, Jacobs P, Lewis J (1989) *AJR Am J Roentgenol* 152:167–173.
24. Panyam J, Labhasetwar V (2003) *Pharmacol Res* 20:212–220.
25. Choi SW, Kim JH (2007) *J Control Rel* 122:24–30.
26. Kong D, Melo LG, Mangi AA, Zhang L, Lopez-Ilasaca M, Perrella MA, Liew CC, Pratt RE, Dzau VJ (2004) *Circulation* 109:1769–1775.
27. Villa AE, Guzman LA, Poptic EJ, Labhasetwar V, D'Souza S, Farrell CL, Plow EF, Levy RJ, DiCorleto PE, Topol EJ (1995) *Circ Res* 76:505–513.

Downloaded at Palestinian Territory, occupied on December 19, 2021

www.manaraa.com